Observation of the Long-Period Monotonic Seismic Waves of the November 11, 2018, Mayotte event by the Iranian Broadband Seismic Stations

Hossein Sadeghi (sadeghi@um.ac.ir)
Ferdowsi University of Mashhad https://orcid.org/0000-0002-7283-3082
Sadaomi Suzuki
Tono Research Institution of Earthquake Science, Association for the Development of Earthquake Prediction

Full paper

Keywords: Mayotte, strange event, monochromatic, long period, Iranian broadband stations

Posted Date: December 4th, 2020

DOI: https://doi.org/10.21203/rs.3.rs-120308/v1

Version of Record: A version of this preprint was published on April 21st, 2021. See the published version at https://doi.org/10.1186/s40623-021-01408-1.

Title page:

Title: Observation of the long-period monotonic seismic waves of the November 11, 2018, Mayotte event by the Iranian broadband seismic stations

Hossein Sadeghi*, Department of Geology, Faculty of Science, Ferdowsi University of Mashhad, Mashhad, Iran, sadeghi@um.ac.ir

Sadaomi Suzuki, *Retired*, Tono Research Institute of Earthquake Science, Association for the Development of Earthquake Prediction, Mizunami, Japan, suzuhome@bcc.bai.ne.jp

***Corresponding author**

Correspondence to Hossein Sadeghi (sadeghi@um.ac.ir)

Abstract

On November 11, 2018, an event generating long-lasting, monotonic long-period surface waves was observed by seismographs around the world. This event occurred at around 09:30 (UTC) east of the Mayotte Island, east Africa. This event is unusual due to the absence of body waves in the seismograms and people's lack of sense. The purpose of this study is to investigate this unusual event using the waveforms recorded by the Iranian National Broadband Seismic Network. The network consisted of 26 stations in operation on November 11, 2018. The stations are located from 4542 km to 5772 km north-northeast of the event's epicentre. The arrival of monochromatic long-period signals is visible around 10 UTC in the recordings of all the stations and lasts for more than 30 minutes. Frequency analysis of the seismograms shows a clear peak at 0.064 Hz (15.6 sec/cycle). The maximum amplitude of the transverse components is less than a half of the radial components. This is in agreement with the theoretical radiation pattern of Rayleigh and Love waves at a frequency of 0.06 Hz from a vertical Compensated Linear Vector Dipole (CLVD) source mechanism. The average apparent phase velocities are calculated as 3.31 km/s and 2.97 km/s, in the transverse and radial

directions, corresponding respectively to the Love and Rayleigh waves in the range of 0.05 to 0.07 Hz. The surface wave magnitude of Ms 5.07 ± 0.22 was estimated. Just before the monochromatic signal, there is some dispersion in the surface waves. This observation may suggest a regular earthquake that triggered the strange Mayotte event.

Keywords

Mayotte, strange event, monochromatic, long period, Iranian broadband stations

Introduction

The 11 November 2018 Mayotte event was first introduced in the media by Wei-Haas (2018) in National Geographic Magazine as a strange earthquake of which seismic waves were recorded by instruments around the world, but unusually nobody felt them. The event occurred at and around 9:30 UTC near offshore of Mayotte Island in the Mozambique Channel between the northern tip of Madagascar and the eastern coast of Africa. The Mayotte Island is one of four main Islands in the volcanic Comoros archipelago. The 11 November Mayotte event in the absence of body waves caused

large, long-lasting, monotonic long-period surface waves travelling around the globe. Before May 2018, the seismic activity of this archipelago was dispersed and moderate with only a few earthquakes with magnitude greater than 4. But in the year following the Mayotte volcano-seismic sequence on May 10, 2018, 32 earthquakes with a magnitude greater than 5 have been recorded (Lemoine et al. 2020). The biggest ever recorded earthquake in the area with Mw 5.9 happened on May 15, 2018 (USGS). Figure 1 shows the recorded waveforms for the May 15, 2018 earthquake, and the Mayotte event at a regional distance station; ABPO (IRIS/IDA seismic network), and at a teleseismic distance station; ASAO (Iranian National Broadband Seismic Network). The epicentres of these two events were located very close to each other, and the epicentral distances are 713 km and 5261 km from ABPO and ASAO stations, respectively. The waveforms show clear differences in the nature of the propagated waves between the regular earthquake and the Mayotte event. The most obvious feature of the Mayotte event is that while large long-period monotonic surface waves are visible, the body waves are absent. The long period waves have appeared for more than 30 minutes both at regional and teleseismic distances. Following Wei-Haas (2018), we

call this event a Strange EarthQuake and abbreviated it as SEQ. A description of this event can be found by underwater volcanic activity. Cesca et al. (2020) suggest drainage of a deep magma reservoir. In this study, we investigate this event using the waveforms recorded by the Iranian National Broadband Seismic Network. The objective of our study is divided into three main categories: Firstly, this event, which is characterized by long-lasting monochromatic, long-period surface waves, will be analyzed by examining its time history and spectral characteristics. The second goal of the research is to estimate the magnitude of the event which is a key parameter for seismic energy emission in the source area. Thirdly, given the increase in pre-event seismic activity, we study the possibility of occurrence of an earthquake just before the event for possible interaction that may trigger the event.

Observation

The broadband seismic network of Iran of the International Institute of Earthquake Engineering and Seismology (IIEES) started operating with 4 stations in 1998 and currently has 31 stations (IIEES 2020). The stations are equipped with Güralp CMG-3T

sensors with a flat velocity response from 120s (0.0083 Hz) to 50 Hz. Twenty six of the stations (triangles in Figure 1) were in operation on November 11, 2018, recording SEQ. The stations are located from 4542 km to 5772 km north-northeast of SEQ's epicentre which was assumed from the study of Lemoine et al. (2020). One and half hour trace view of the vertical component of the broadband records filtered between 0.01 and 0.1 Hz, and the frequency spectra of their unfiltered waveforms are displayed in Figure 2. All the stations show clear long-period seismic waves arriving around 10:00 UTC on November 11, 2018, and frequency analysis of the seismograms shows a clear peak in the spectral amplitudes. The peak is in a narrow frequency band of 0.05 to 0.07 Hz. Among the stations, no significant changes are observed in the monochromatic wave trains and the narrow-band spectral peak.

Seismic waves and focal mechanisms

We compared the seismic waves of SEQ and the largest regular earthquake (called May 15 in Figure 1 and this text). Figure 3 shows their seismic waves of the three components observed at ASAO station. The ground noise level of ASAO station is low.

91 It is clear that the observed waveforms of the two earthquakes differ greatly even
92 though the epicentres are close. The SEQ waveforms are dominated by long-lasting
93 monochromatic surface waves. And there is no signal of body waves. The maximum
94 amplitude of the transverse component is less than a half of the radial component. While
95 clear P and S phase arrivals are observed on the May 15 seismograms, and dispersion of
96 the surface waves clearly appears in all three components on the seismograms. The
97 maximum amplitude of the transverse component is 1.2 times of the radial component.
98 Figure 4(a) displays focal mechanisms of SEQ and May 15. Beach-ball representation
99 of the best fitting moment tensors for them are shown. The focal mechanism of May 15
100 indicates dominant strike-slip with NW-SE directed compression. While the moment
101 tensor for SEQ, as discussed in Cesca et al. (2020), can be introduced by vertical
102 Compensated Linear Vector Dipole (CLVD). Previous studies discussed the relation
103 between active volcanism and the occurrence of rarely observed non-double-couple
104 earthquakes (e.g. Shuler et al. 2013a, and b). They introduced possible physical
105 mechanisms for the vertical-CLVD earthquakes and their unusual seismic radiation
106 pattern and frequency content. The manifestation of SEQ is the presence of surface

107 waves in the absence of body waves. In a vertically symmetric CLVD, it is expected no
108 love waves and no azimuthal variations in Rayleigh waves, but the focal mechanism of
109 the SEQ shows no vertical symmetry axes. Comparing with the regular earthquake we
110 have to make a model for radiation pattern of the surface waves considering the moment
111 tensors. Figure 4(b) shows the theoretical seismic energy radiation pattern of Rayleigh
112 and Love waves at a frequency of 0.06 Hz. The spectral amplitudes based on the
113 considered source mechanism were calculated in the azimuthal spacing of 1° by using
114 the data product (Rösler et al. 2020) of the IRIS DMC's Surface-Wave Radiation
115 Pattern. Seismic radiation for the SEQ is dominated by Rayleigh waves displaying a
116 nearly oval form with larger elongation in northeast-southwest direction. Love waves
117 are clearly less energetic than Rayleigh waves and show more azimuthal variation in the
118 maximum amplitude. Seismic radiation for May 15 shows larger spectral amplitudes for
119 Love waves than Rayleigh waves. The spatial variation of maximum amplitude shows a
120 clear four-lobe pattern for Love waves, while for the Rayleigh waves the radiation
121 pattern has a two-lobe shape. The broadband station in Iran locates in the azimuth range
122 of 359 to 21 degrees from SEQ, which lie nearly close to the maximum radiation of

surface waves.

Figure 5 presents the spectrograms of power spectral density (PSD) in $(m/sec)^2/Hz$, Fourier spectra, and dominant periods of the SEQ and May 15 vertical and transverse components at ASAO station (the seismograms are shown in Figure 3). As we expected from the model of radiation pattern for SEQ, the surface waves in the vertical components (dominated by Rayleigh waves) have larger amplitudes than the transverse component (Love waves). Besides, SEQ shows four clear differences with the regular earthquakes. The first obvious difference is the very long-lasting of its surface waves. The second difference can be seen through the spectrograms that a dominant monochromatic surface waves (around 0.06 Hz) extending throughout the signal duration. The Fourier spectra show a clear large peak at 0.064 Hz. The third and fourth differences can be observed in the graph of the dominant period over time; the constant dominant period for the transverse component is lower than the vertical component, and the signals in both components propagate with the nearly same velocity. A convergence of surface wave velocities can be seen also in the graph of the dominant period for May 15 around a period of 16 seconds, which corresponds to the Airy phase with a minimum

139 in the group velocity dispersion curves (Bullen and Bolt, 1985). The Airy phases in the
140 transverse component can be observed by large amplitudes after an abrupt termination
141 in the wave trains (see Figure 3, bottom). The gap between red lines around 1700 sec in
142 the dominant period graph for the transverse component is due to this termination, and
143 also our criteria to select the power values greater than the mean value of PSD.
144

145 Group velocities of the surface waves

146 We used two analysis methods, frequency-wavenumber (f-k) analysis and regression
147 analysis, to estimate the group velocity of the SEQ surface waves. We applied f-k
148 analysis to a group of 9 relatively closely spaced stations as an array using the python
149 library Obspy (Beyreuther et al. 2010). The selected stations were marked by red
150 triangles in the map of Figure 1. The array response function for the directional
151 sensitivity and its resolution power is shown in Figure 6. This function is computed for
152 a frequency band of 0.05-0.07 Hz. There is no distinct side lobe in the array response.
153 The semblance technique (Neidell and Taner, 1971) was used to measure slowness and
154 back azimuths of the coherent wave phases that crossed the array. The analysis was

155 applied to 1-hour sections from 2018-11-11T09:45:00 to 2018-11-11T10:45:00. After
156 the waveform data were filtered using a bandpass filter of 0.05–0.07 Hz, the semblance
157 coefficient was calculated for a sliding window length of 20 s and 1 s for steps. The
158 range of slowness is searched from 0.1 to 1.5 s/km in steps of 0.05 s/km. The quality of
159 the stacked signal is measured by the semblance coefficient, which is a dimensionless
160 quantity between 0 and 1 for no coherency and perfect coherency, respectively. The
161 semblance values show a coherency peak at about 75 per cent for the radial (Rayleigh
162 waves) components (Figure 7a). But for the transverse (Love waves) components, the
163 semblance values do not show a unique peak and coherency higher than 55 per cent
164 (Figure 7b). For the regression analysis, we manually picked the wave group arrivals on
165 bandpass filtered radial and transverse components of all 26 stations. A station was
166 assumed as a reference and the delays or advances in arrival times of the other stations
167 from the reference were calculated. The apparent velocity and back azimuth were
168 estimated by fitting a plane wave, a straight line through the least regression. The
169 procedure was repeated by applying another station as the reference. The averages of
170 the apparent velocities were calculated for transverse and radial as 3.31 and 2.97

171 km/sec, respectively. They correspond with the phase velocities of Love wave and
172 Rayleigh wave, respectively, in the frequency band of 0.05–0.07 Hz. Figure 8 shows the
173 average back azimuth (black arrows). They are generally in good agreement with the
174 back azimuth to the SEQ epicentre (red arrows).
175

176 Estimation of magnitudes

177 Using seismic data of the 26 Iranian seismic stations we estimated the surface wave
178 magnitudes (*Ms*) of SEQ and the regular earthquakes occurring around Mayotte Island.
179 We used the equation (1) named the Prague formula (Karnik et al.1962; Vanek et al.
180 1962).

181 $$Ms = \log(A/T) + 1.66 \log \Delta + 3.30 \qquad (1)$$

182 Where A is the peak amplitude of the surface waves in micrometre, T is the period in
183 second, and Δ is the epicentral distance in degree. First, the surface wave magnitude of
184 SEQ was calculated to be $Ms = 5.07 \pm 0.22$. Secondly, we calculated the surface wave
185 magnitudes of the 24 regular earthquakes with body wave magnitudes (*mb* presented by
186 USGS) >4.5 occurring from May 13 to June 1, 2018. The surface wave magnitudes for

187 the selected events were calculated using averages of 10 amplitude readings at least.

188 Those surface wave magnitudes (*Ms*) and body wave magnitudes (*mb*) are listed in

189 Table Appendix. It is important to notice that the *mb*=5.8 is the biggest earthquake and

190 the lower limit of *mb*=4.5 was defined based on the signal strength and quality for

191 reliable amplitude measurements. And we compared the relationship between *Ms* and

192 *mb* as shown in Figure 9. Assuming that the best regression equation between *Ms* and

193 *mb* is fitted in the form of $mb=a+bMs$, we obtained the following equation (eq. 2):

194 $$mb=2.54\ (\pm\ 0.29)+0.56(\pm\ 0.07)Ms, \quad \text{std}=0.15, \quad R^2=0.76 \qquad (2)$$

195 Equation 2 shows that the average of *Ms* in a range of 4.5 to 5.8 is 0.5 to 0 lower than

196 *mb* in average. Scordilis (2006) studied empirical global relations for magnitude scales

197 conversions and found nearly same result for $Ms< 6.2$. We defined converted body wave

198 magnitude *mb(conv)* using the following equation (3),

199 $$mb(conv) \equiv 2.54 + 0.56Ms \qquad (3)$$

200 Obtained *mb(conv)* listed in Table 1 for the three largest earthquakes and SEQ. The

201 hypocenters of the three regular earthquakes were referred from USGS, while the

202 location of SEQ was assumed from the source location which best fitted to the ground

deformation after the early July 2018 by Lemoine et al. (2020).

A trigger earthquake just before SEQ

Lemoine et al. (2020) claimed that there were no strong earthquakes precede the SEQ event, but some earthquakes are embedded, especially at the beginning of the monochromatic SEQ signal. Here, we want to take a closer look at the beginning of the signal to investigate the possibility of an earthquake occurring before SEQ. If so, it could be a trigger earthquake of SEQ. Figure 10 shows the waveform and time variation of the dominant period at ASAO station for the vertical component of SEQ. It is clear from the figure that immediately before the arrival of the long-lasting monochromatic signal of SEQ, the surface waves (Rayleigh waves) are dispersed. The period decreases from 17.5 seconds to 16 seconds, during the time from 09:56:56 to 09:58:38 (UTC), for about 100 seconds as shown in Figure 10(b). It could correspond to the occurrence of a regular earthquake just before the SEQ event. We call this event as Just Before the monochromatic Event (JBE) in this paper. Comparing with arriving time of the equivalent dominant periods of the regular earthquakes (listed in Table 1) that occurred

219 in the vicinity of SEQ, the origin time of the JBE was estimated at UTC time of
220 09:27:56 ± 13 sec. The surface wave magnitude of Ms=4.3 ± 0.11 was calculated for
221 JBE. Cesca et al. (2019) detected a volcano-tectonic earthquake on 11 November 2018,
222 09:27:59.575 at latitude 12.8058 °S and longitude 45.4736 °E. They determined its
223 magnitude based on a regional moment tensor inversion following the record of a single
224 strong-motion station on Mayotte as *Mw* 3.8. This earthquake must be JBE. Now, the
225 question is how long before SEQ, did it occur? An answer can be obtained by
226 comparing the frequency content of these two events. Figure 10 (b) shows that the
227 dominant period line of JBE is bent at around 16-sec period at 09:58:38 UTC (red
228 arrow). It may suggest that the surface wave of JBE lasted until at least 09:58:38 UTC.
229 For more accurate judgment, we applied a notch (a band-stop with narrow stopband)
230 filter to separate the two merged events. In the spectrum of SEQ, the largest peak is at
231 15.6 sec. Therefore, we filtered out the 15.6-sec signal from the waveform using the
232 notch filter to remove the main component of the signal of SEQ. The result is shown in
233 Figure 10 (c). This figure shows that the filter removed the main content of the
234 waveform corresponding to the long duration monochromatic signal of SEQ after

09:59:09 UTC (black arrow). It suggests that the surface wave of SEQ arrived at latest 09:59:09 UTC. When we assume that the difference in surface wave velocity between the periods of 15.6-sec and 16-sec is nearly the same, the time difference between 09:58:38 UTC and 09:59:09 UTC may suggest that JBE occurred less than 31 sec before the start of SEQ.

Conclusions

We have studied the Mayotte strange event (called SEQ), on November 11, 2018, using the records of the Iranian National broadband seismic network. The long-lasting, monotonic long-period surface waves are visible and dominate the waveforms. The frequency of the monochromatic signals is 0.064 Hz. The radiation pattern of the surface waves supports a vertical Compensated Linear Vector Dipole (CLVD) source mechanism. The apparent phase velocities of 3.31 km/s and 2.97 km/s respectively for the Love and Rayleigh waves of the event were obtained from the results of our array analysis. The surface magnitude (*Ms*) of SEQ was estimated to be *Ms* 5.1. Evidence of dispersion in surface waves just before the arrival of the monochromatic event,

suggesting the possibility that SEQ might be triggered by a regular earthquake (called JBE). The origin time and magnitude of JBE were estimated around 09:28 (UTC) and *Ms* = 4.3.

Declarations

Ethics approval and consent to participate

Not applicable

Consent for publication

Not applicable

List of abbreviations

Compensated Linear Vector Dipole (CLVD), Strange EarthQuake (SEQ), International Institute of Earthquake Engineering and Seismology (IIEES), Power Spectral Density (PSD), frequency-wavenumber (f-k), converted body wave magnitude (*mb(conv)),* Just Before the monochromatic Event (JBE)

Availability of data and materials

The waveform data are available by request to International Institute of Earthquake Engineering and Seismology (IIEES).

Competing interests

The authors declare that they have no competing interests.

Funding

No funding was obtained for this study and for preparation of this paper.

Authors' contributions

H.S. performed the data analysis and result evaluation, and drafted the manuscript. S.S. contributed to the interpretation of the results and involved in drafting the manuscript for intellectual content.

Acknowledgement

The authors are very thankful to O. Murakami for valuable discussions and guidance as well as to G. Javan Doloei and A. Ashari for sending us the seismic waveform data of IIEES network, and also A. Lemoine for providing us the Bertil et al. (2019) catalogue of the Mayotte region seismicity. The seismic data of ABPO station used in this study was obtained from IRIS/IDA seismic network II (http://dx.doi.org/doi:10.7914/SN/II). Some figures were made using the GMT (Wessel and Smith, 1998) software package.

Authors' information

Hossein Sadeghi is associate professor at Department of Geology, Faculty of Science, Ferdowsi University of Mashhad, Iran.

Sadaomi Suzuki is retired from Tono Research Institute of Earthquake Science, Association for the Development of Earthquake Prediction, Mizunami, Japan,

References

Bertil D, Roullé A, Lemoine A, Colombain A, Hoste-Colomer R, Gracianne C, Meza-Fajardo K, Maisonhaute E, Dectot G (2019) MAYEQSwarm2019: BRGM earthquake catalogue for the Earthquake Swarm located East of Mayotte.2018 May 10th - 2019 May 15th. Available at dataBRGM. https://doi.org/10.18144/rmg1-ts50. Accessed 18 Nov 2020

Beyreuther M, Barsch R, Krischer L, Megies T, Behr Y, Wassermann J (2010) ObsPy: a python toolbox for seismology. Seismol Res Lett 81:530–533

Bullen KE, Bolt BA (1985) Introduction to the Theory of Seismology. Cambridge University, Cambridge

Karnik V, Kondorskaya N, Riznichenko J, Savarenski E, Solovyov S, Shebalin N, Vanek, J, Zatopel A (1962) Standardisation of the earthquake magnitude scale. Studia Geophys Geodet 6:41–47

Cesca S, Heimann S, Letort J, Razafindrakoto HNT, Dahm T, Cotton F (2019) Seismic catalogues of the 2018-2019 volcano-seismic crisis offshore Mayotte, Comoro Islands. V. 1.0 (October 2019). Available at GFZ Data Services. http://doi.org/10.5880/GFZ.2.1.2019.004. Accessed 18 Nov 2020

Cesca S, Letort J, Razafindrakoto HNT, Heimann S, Rivalta E, Isken MP, Nikkhoo M, Passarelli L, Petersen GM, Cotton F, Dahm T (2020) Drainage of a deep magma reservoir near Mayotte inferred from seismicity and deformation. Nat Geosci 13(1): 87–93. doi.org/10.1038/s41561-019-0505-5.

316

317 IIEES (2020). International Institute for Earthquake Engineering and Seismology

318 (IIEES). http://www.iiees.ac.ir. Accessed 18 Nov 2020

319

320 Lemoine A, Briole P, Bertil D, Roullé A, Foumelis M, Thinon I, Raucoules D,

321 Michele M, Valty P, Colomer RH (2020) The 2018–2019 seismo-volcanic crisis east of

322 Mayotte, Comoros islands: seismicity and ground deformation markers of an

323 exceptional submarine eruption. Geophys J Int 223(1): 22-44.

324 doi.org/10.1093/gji/ggaa273

325

326 Wei-Haas M(2018) Strange waves rippled around the world, and nobody knows why.

327 Natl. geogr. mag., published November 28, 2018.

328

329 Neidell NS, Taner MT (1971) Semblance and other coherency measures for

330 multichannel data. Geophysics 36(3): 482–497. doi.org/10.1190/1.1440186

331

Rösler B, van der Lee S (2020) Using Seismic Source Parameters to Model Frequency-Dependent Surface-Wave Radiation Patterns. Seismol. Res. Lett 91:992–1002. doi:10.1785/0220190128

Scordilis EM (2006) Empirical global relations converting MS and mb to moment magnitude. J Seismol 10:225–236

Shuler A, Ekstrom G, Nettles M (2013a) Physical mechanisms for vertical-CLVD earthquakes at active volcanoes. J Geophys Res 118, 1569–1586. doi:10.1002/jgrb.50131

Shuler A, Ekstrom G, Nettles M (2013b), Global observation of vertical-CLVD earthquakes at active volcanoes, J Geophys Res 118:138–164. doi:10.1029/2012JB009721

Vaněk J, Zapotek A, Karnik V, Kondorskaya NV, Riznichenko YV, Savarensky EF,

348 Solov'yov SL, Shebalin NV (1962) Standardization of magnitude scales. Izvestiya
349 Akad. SSSR Ser Geofiz 2:153-158
350
351 Wessel P, Smith WHF (1998) New improved version of Generic Mapping Tools
352 released. EOS Trans. Am. Geophys. Union 79: 579-579
353
354
355 **Figure Legends**
356 Figure 1. Left) The map area of the November 11, Mayotte event (called SEQ), and
357 locations of the Iranian broadband seismic stations (triangles) are shown. The red
358 triangles show the selected stations that were used for array analysis. The enlarged map
359 view shows the locations of the biggest regular earthquake (black star behind red star),
360 Mw 5.9 of May 15, 2018 (USGS), and the SEQ (red star) (Lemoine et al. 2020). The
361 seismic waves of the two events recorded by ABPO (IRIS/IDA seismic network) in left
362 and by ASAO (Iranian National Broadband Seismic Network) in right. The blue links
363 indicate great circles connecting the epicentre and ABPO station which located at SSE
364 about 6.4 degrees from the events and ASAO station which located at NNE about 47.5

365 degrees from the events. The length of seismograms is 4000 s and their start time is
366 labelled, which corresponds to the origin time of the May 15 event at 15:48:08 (UTC),
367 and for the SEQ at 09:30:00 (UTC). The waveforms are vertical components and have
368 been filtered in the range of 0.01-0.1 Hz.
369
370 Figure 2. One and a half hour trace view of the vertical components of the 26 Iran's
371 broadband stations. The traces are ordered from top to bottom by increasing epicentral
372 distance (station name and epicentral distance are displayed). The waveforms are band-
373 passed filtered between 0.01 and 0.1 Hz. long-lasting, long-period seismic waves are
374 observed arriving at around 10:00 UTC on November 11, 2018. The right-hand figures
375 are the Fourier spectra of their unfiltered seismograms. The peak of spectra (indicated by
376 the grey arrow in the two bottom spectra) is at 0.064 Hz (15.6 sec/cycle).
377
378 Figure 3. Comparison of the vertical, radial, and transverse components for the SEQ (top)
379 and May 15 (bottom) events observed at station ASAO. The waveforms show 45 minutes
380 and filtered between 0.01 and 0.1 Hz by using a fourth-order Butterworth filter. Vertical

381 short lines in the waveforms in bottom show the arrivals of P or S phase.

382

383 Figure 4. (a) Focal mechanisms of the SEQ (top) and May 15 (bottom) events. The SEQ
384 moment tensor (MT) is defined by averaging the MTs of 21 events with long-duration
385 monochromatic, very long period signals (VLP) that provided in the seismic catalogues
386 of the 2018-2019 crises of the east of Mayotte Island by Cesca et al. (2019). The VLP
387 MTs show vertical-CLVD, while the focal mechanism of May 15 (from GCMT
388 catalogue) indicates dominant strike-slip faulting with NW-SE directed P-axis and NE-
389 SW directed T-axis. (b) The azimuthal radiation pattern for surface waves at a frequency
390 of 0.06 Hz considering the moment tensors of the SEQ (top) and May 15 (bottom) events.
391 The black circles show the relative spectral displacement amplitude in a linear scale for
392 each pair of Rayleigh and Love waves. The red arrow points to station ASAO.

393

394 Figure 5. Spectrograms of the power spectral density (PSD) in vertical component (right-
395 top) and transverse component (right-bottom), Fourier spectra (left-top) and the dominant
396 periods over time (left-bottom) of the vertical (Z) and transverse (T) components of

397 ASAO station for SEQ (a) and May 15 (b). The dominant periods are plotted by dots and
398 the line is a piecewise linear interpolation through the data points. Note that, the periods
399 with power less than the mean values of the spectrogram are removed from the graph.
400 The grey circle on the Fourier spectra of May 15 indicates a peak of around 0.06 Hz
401 related to the Airy phase of surface waves. This peak is also clearly displayed by the
402 maximum values of PSD on the spectrograms of transverse components.
403
404 Figure 6: Array response function at 0.05-0.07 Hz. The colour scheme corresponds to the
405 normalized amplitude of the relative power, as shown by colour bar on the right.
406
407 Figure 7. The semblance values, back azimuth in degree, and apparent slowness in s/km
408 for radial components (a) and transverse components (b) of the SEQ are shown. The data
409 of 9 array stations (red triangles in Figure 1) were used. A pair of vertical grey lines in
410 (a) indicates the solution with the maximum semblance value of 0.75 per cent.
411
412 Figure 8: The estimated back azimuth (black arrow) at each station using both Rayleigh

413 and Love waves of SEQ (see text). Red arrow shows the direction to the epicentre of SEQ

414 in each station.

415

416 Figure 9. Relation between the calculated surface wave magnitude and the body wave

417 magnitude estimated by USGS

418

419 Figure 10. (a) is the same as the latter half of the top of Figure 3. Waveforms of JBE (Just

420 Before the monochromatic Event) and SEQ can be seen. (b) shows the dominant periods

421 of the waveforms in figure (a). The dispersion of the surface waves is clear, and in the

422 range of periods from 17.5 to 16.5 sec is visible in the waveform (marked by red). The

423 red arrow indicates 09:58:38 UTC. (c) shows notch filter output of the waveform with the

424 notch in the period of 15.6 sec and the bandwidth of 1 sec. The black arrow indicates

425 09:59:09 UTC.

426

427

428 **Table Legend**

429 Table 1. The hypocenter location and magnitudes (mb, Ms, and mb(conv)) for three

430 largest earthquakes, occurring during May 2018, SEQ and JBE on November 11, 2018

*No** or name	*Date* Year-Month-Day	*Hypocenter*				*Magnitude*		
		Origin Time (UTC)	*Location*			*mb*	*Ms*	*mb(conv)*
			Lat.(°S)	*Lon. (°E)*	*Depth (km)*			
19	*2018-05-15*	*15:48:09*	*12.776*	*45.581*	*17*	*5.8*	*5.6*	*5.7*
15	*2018-05-20*	*08:01:27*	*12.798*	*45.668*	*10*	*5.3*	*5.0*	*5.3*
14	*2018-05-21*	*00:47:14*	*12.850*	*45.654*	*10*	*5.5*	*5.1*	*5.4*
SEQ	*2018-11-11*	*~09:28*	*12.777*	*45.590*	*28*	*-*	*5.1*	*5.4*
JBE	*2018-11-11*	*~09:28*	*12.777?*	*45.590?*	*28?*	*-*	*4.3*	*4.9*

431 **This is the number of the regular earthquakes listed in Appendix*

432

Figures

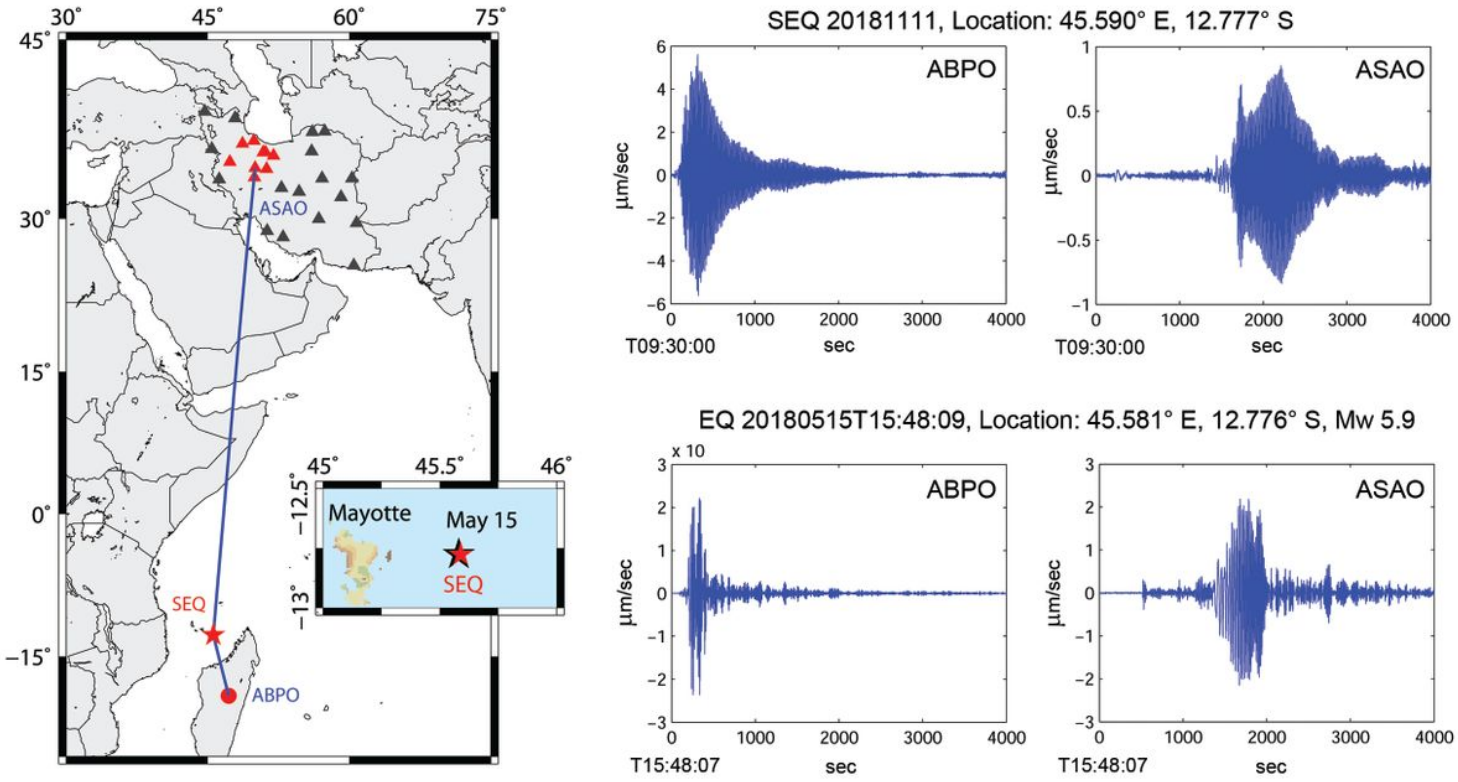

Figure 1

Left) The map area of the November 11, Mayotte event (called SEQ), and locations of the Iranian broadband seismic stations (triangles) are shown. The red triangles show the selected stations that were used for array analysis. The enlarged map view shows the locations of the biggest regular earthquake (black star behind red star), Mw 5.9 of May 15, 2018 (USGS), and the SEQ (red star) (Lemoine et al. 2020). The seismic waves of the two events recorded by ABPO (IRIS/IDA seismic network) in left and by ASAO (Iranian National Broadband Seismic Network) in right. The blue links indicate great circles connecting the epicentre and ABPO station which located at SSE about 6.4 degrees from the events and ASAO station which located at NNE about 47.5 degrees from the events. The length of seismograms is 4000 s and their start time is labelled, which corresponds to the origin time of the May 15 event at 15:48:08 (UTC), and for the SEQ at 09:30:00 (UTC). The waveforms are vertical components and have been filtered in the range of 0.01-0.1 Hz. Note: The designations employed and the presentation of the material on this map do not imply the expression of any opinion whatsoever on the part of Research Square concerning the legal status of any country, territory, city or area or of its authorities, or concerning the delimitation of its frontiers or boundaries. This map has been provided by the authors.

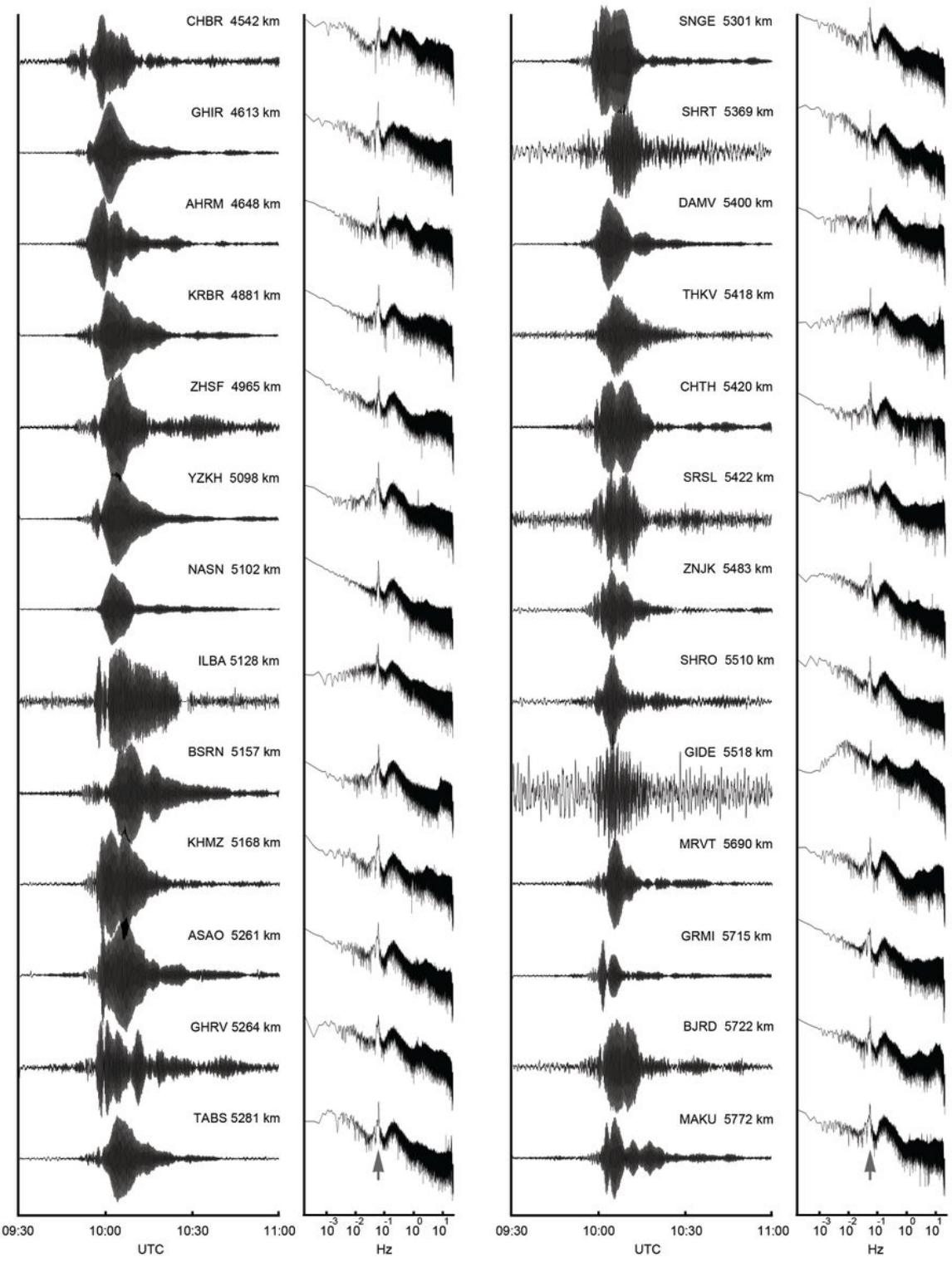

Figure 2

One and a half hour trace view of the vertical components of the 26 Iran's broadband stations. The traces are ordered from top to bottom by increasing epicentral distance (station name and epicentral distance are displayed). The waveforms are band-passed filtered between 0.01 and 0.1 Hz. long-lasting, long-period seismic waves are observed arriving at around 10:00 UTC on November 11, 2018. The right-hand

figures are the Fourier spectra of their unfiltered seismograms. The peak of spectra (indicated by the grey arrow in the two bottom spectra) is at 0.064 Hz (15.6 sec/cycle).

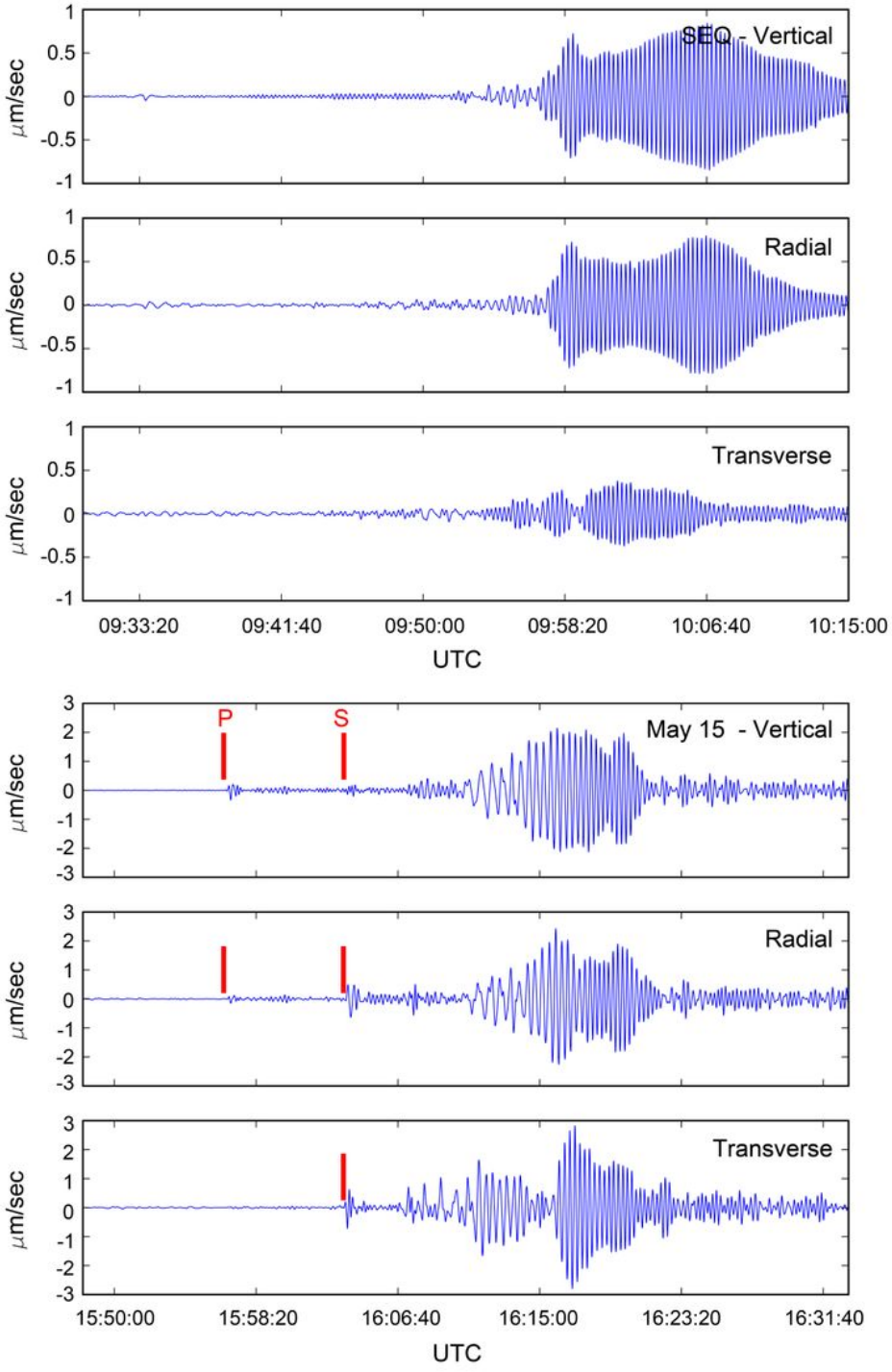

Figure 3

Comparison of the vertical, radial, and transverse components for the SEQ (top) and May 15 (bottom) events observed at station ASAO. The waveforms show 45 minutes and filtered between 0.01 and 0.1 Hz

by using a fourth-order Butterworth filter. Vertical short lines in the waveforms in bottom show the arrivals of P or S phase.

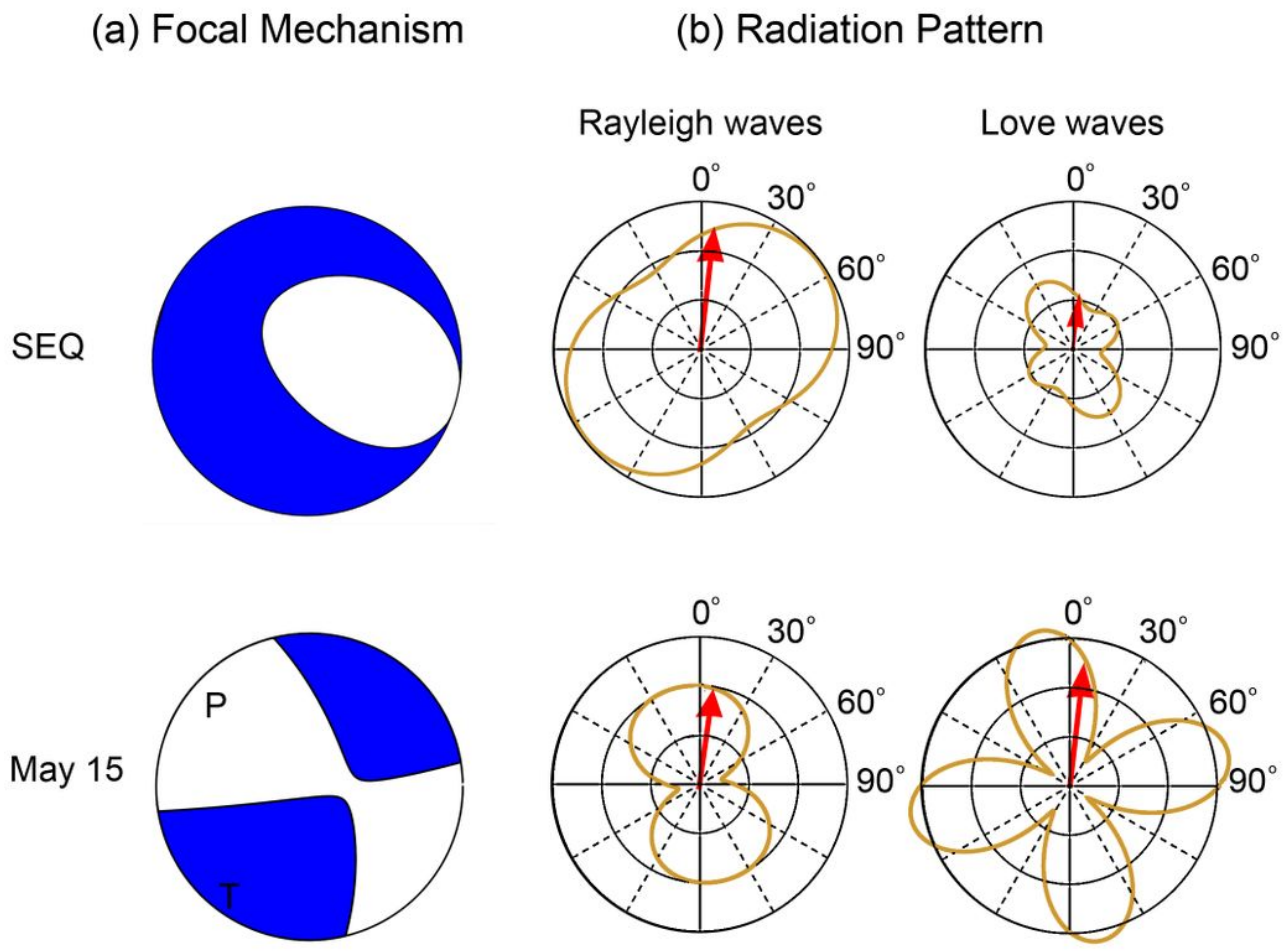

Figure 4

(a) Focal mechanisms of the SEQ (top) and May 15 (bottom) events. The SEQ moment tensor (MT) is defined by averaging the MTs of 21 events with long-duration monochromatic, very long period signals (VLP) that provided in the seismic catalogues of the 2018-2019 crises of the east of Mayotte Island by Cesca et al. (2019). The VLP MTs show vertical-CLVD, while the focal mechanism of May 15 (from GCMT catalogue) indicates dominant strike-slip faulting with NW-SE directed P-axis and NE-SW directed T-axis. (b) The azimuthal radiation pattern for surface waves at a frequency of 0.06 Hz considering the moment tensors of the SEQ (top) and May 15 (bottom) events. The black circles show the relative spectral displacement amplitude in a linear scale for each pair of Rayleigh and Love waves. The red arrow points to station ASAO.

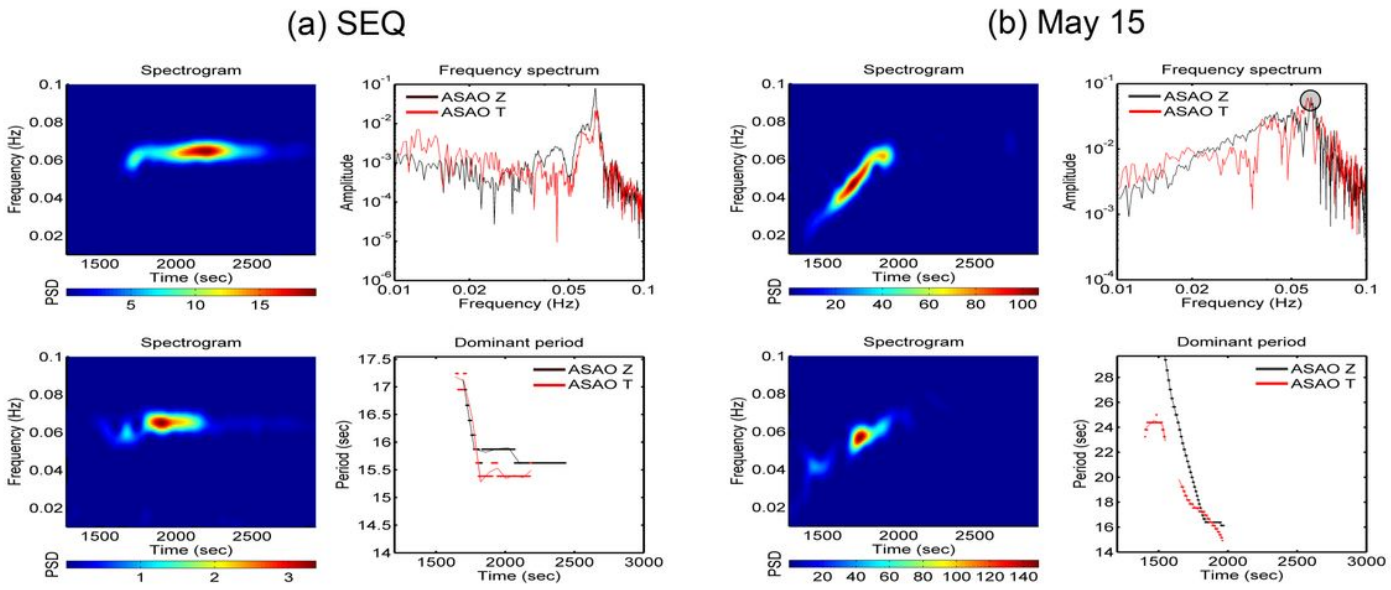

Figure 5

Spectrograms of the power spectral density (PSD) in vertical component (right-top) and transverse component (right-bottom), Fourier spectra (left-top) and the dominant periods over time (left-bottom) of the vertical (Z) and transverse (T) components of ASAO station for SEQ (a) and May 15 (b). The dominant periods are plotted by dots and the line is a piecewise linear interpolation through the data points. Note that, the periods with power less than the mean values of the spectrogram are removed from the graph. The grey circle on the Fourier spectra of May 15 indicates a peak of around 0.06 Hz related to the Airy phase of surface waves. This peak is also clearly displayed by the maximum values of PSD on the spectrograms of transverse components.

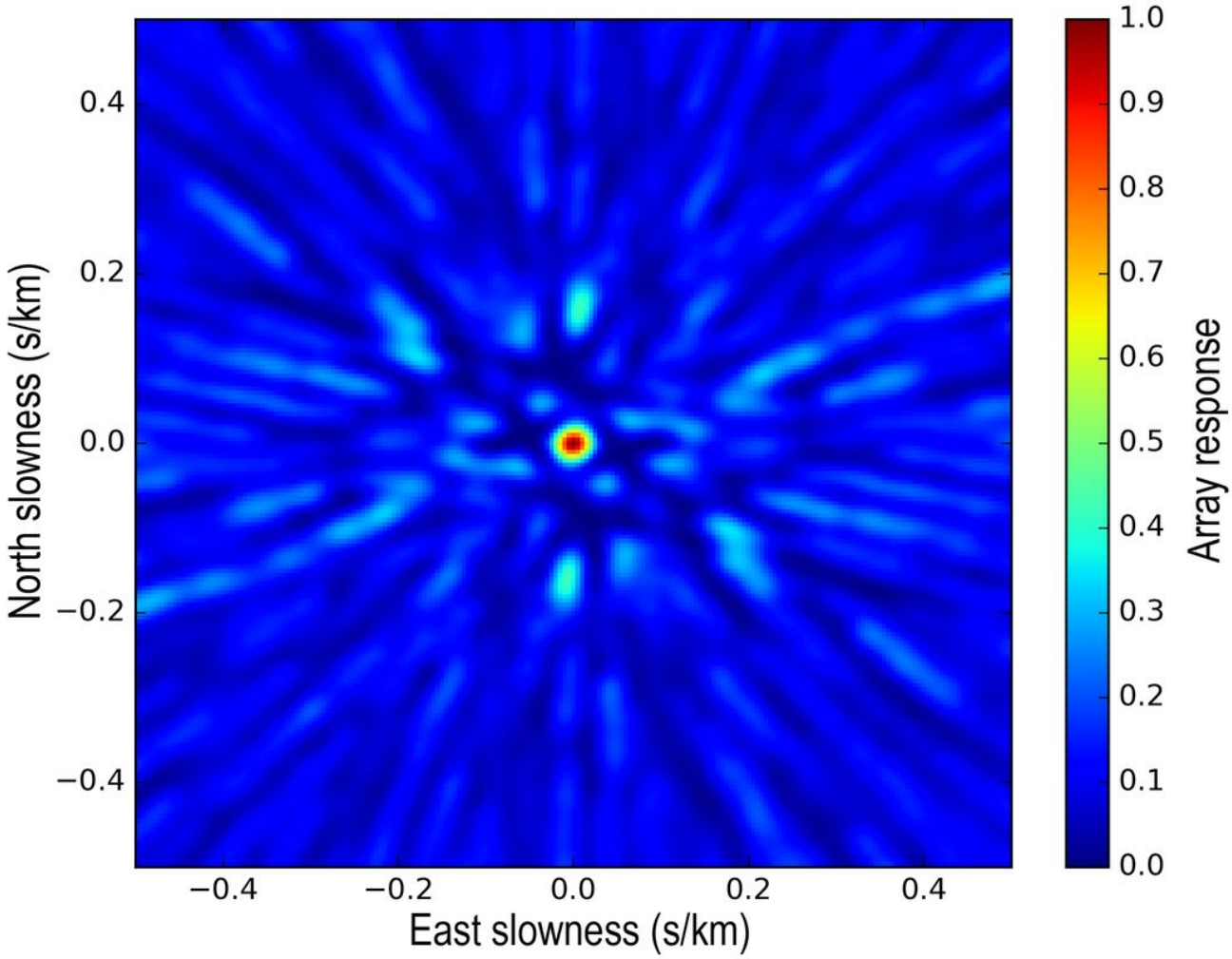

Figure 6

Array response function at 0.05-0.07 Hz. The colour scheme corresponds to the normalized amplitude of the relative power, as shown by colour bar on the right.

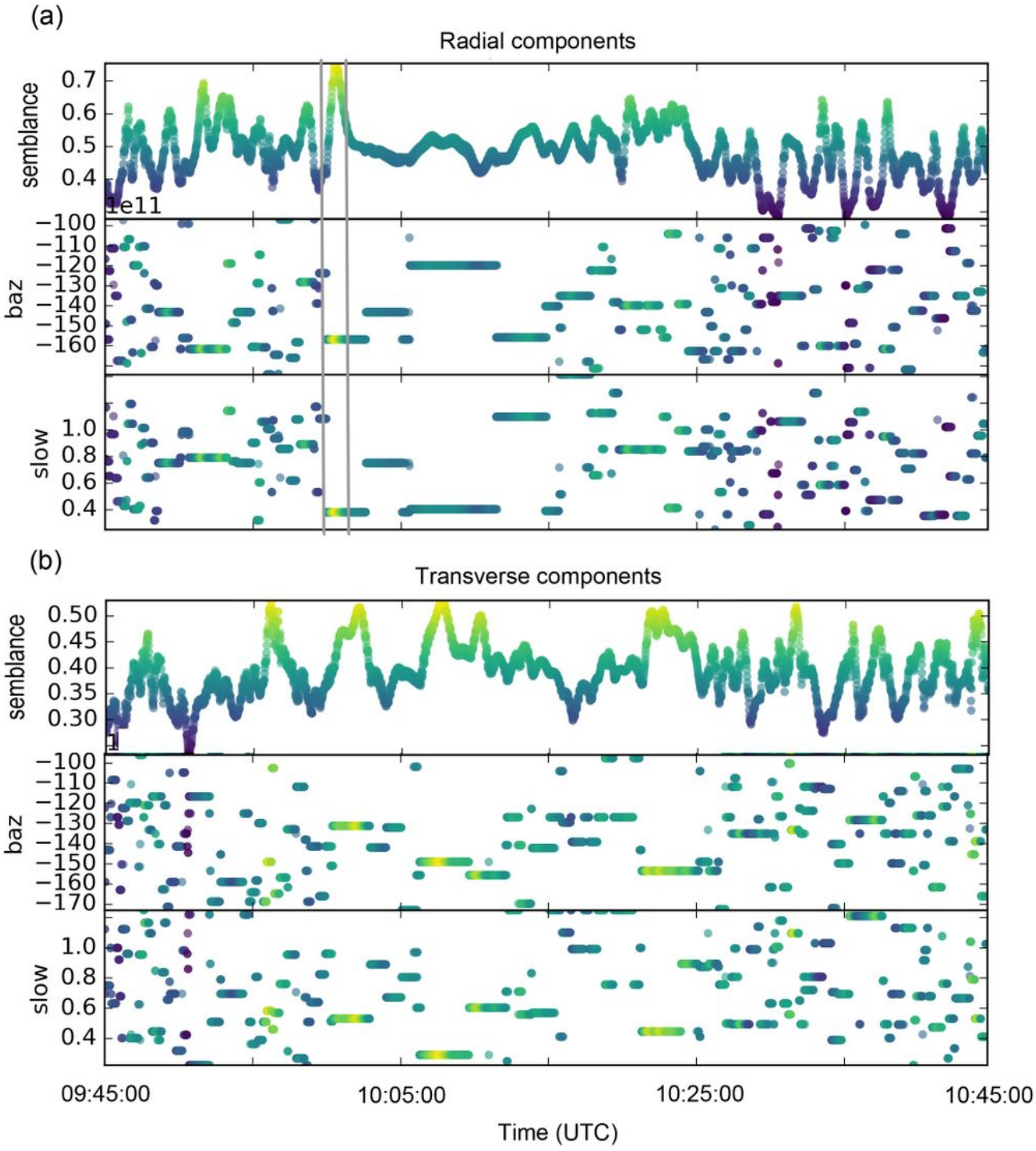

Figure 7

The semblance values, back azimuth in degree, and apparent slowness in s/km for radial components (a) and transverse components (b) of the SEQ are shown. The data of 9 array stations (red triangles in Figure 1) were used. A pair of vertical grey lines in (a) indicates the solution with the maximum semblance value of 0.75 per cent.

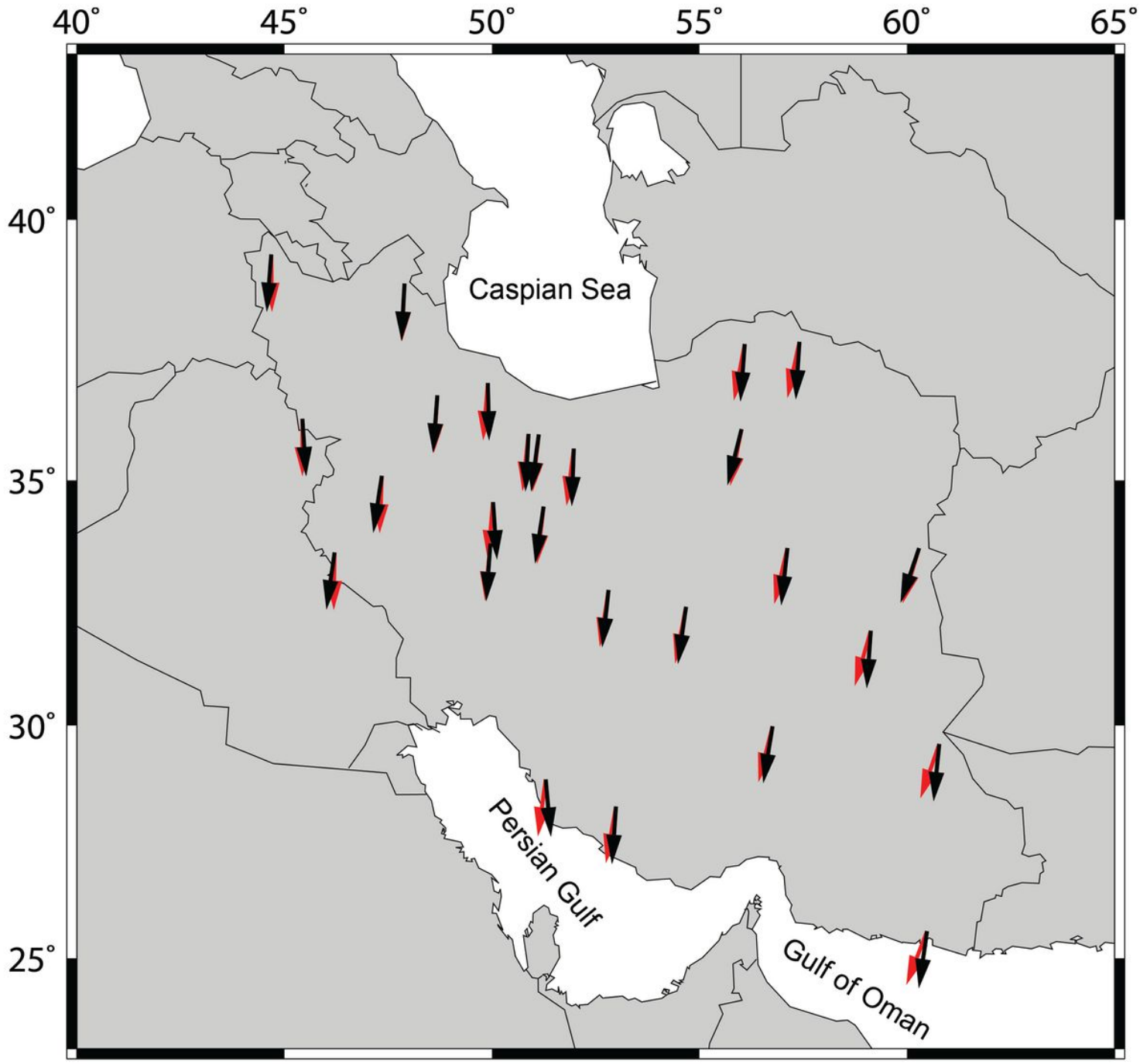

Figure 8

The estimated back azimuth (black arrow) at each station using both Rayleigh and Love waves of SEQ (see text). Red arrow shows the direction to the epicentre of SEQ in each station. Note: The designations employed and the presentation of the material on this map do not imply the expression of any opinion whatsoever on the part of Research Square concerning the legal status of any country, territory, city or area or of its authorities, or concerning the delimitation of its frontiers or boundaries. This map has been provided by the authors.

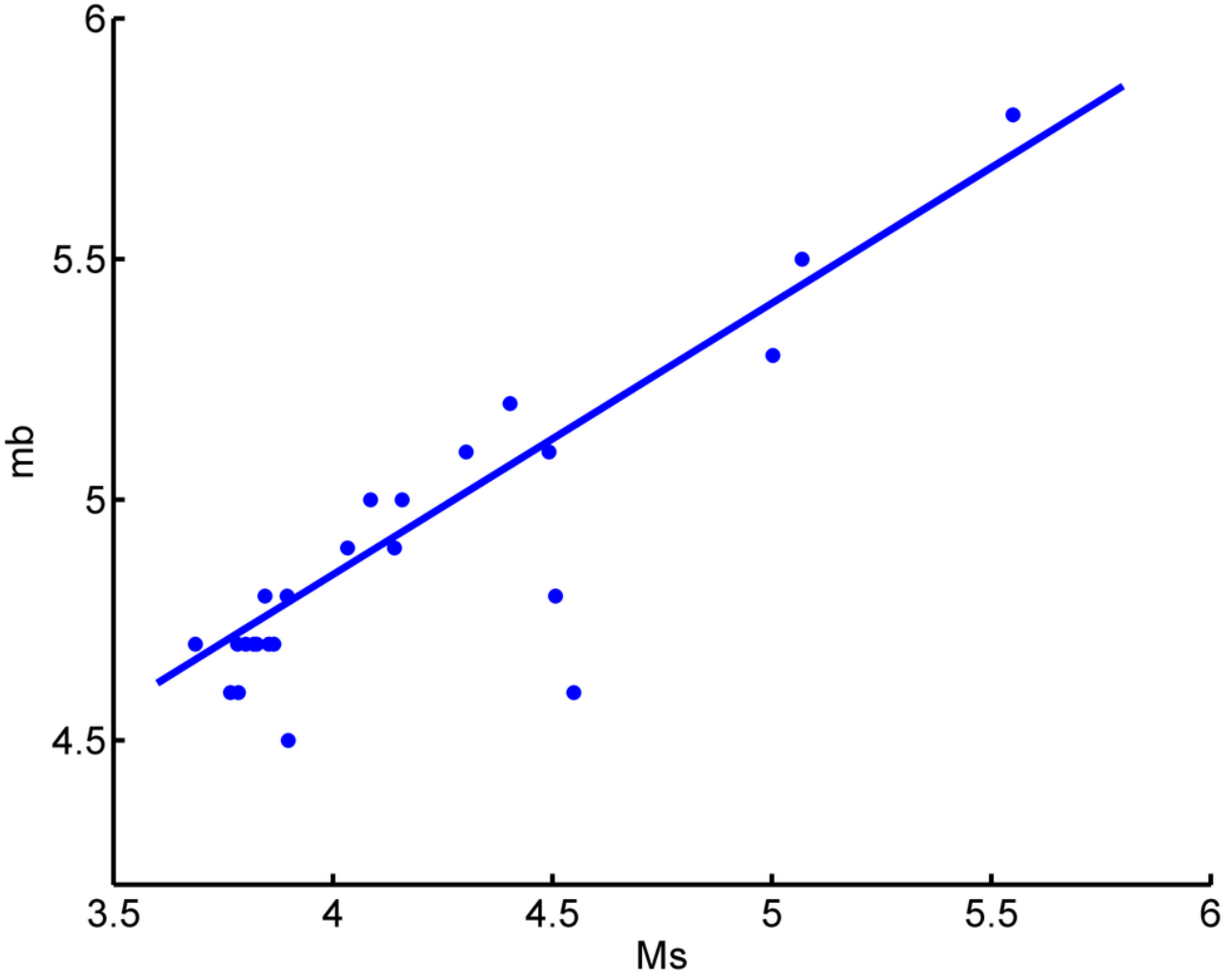

Figure 9

Relation between the calculated surface wave magnitude and the body wave magnitude estimated by USGS

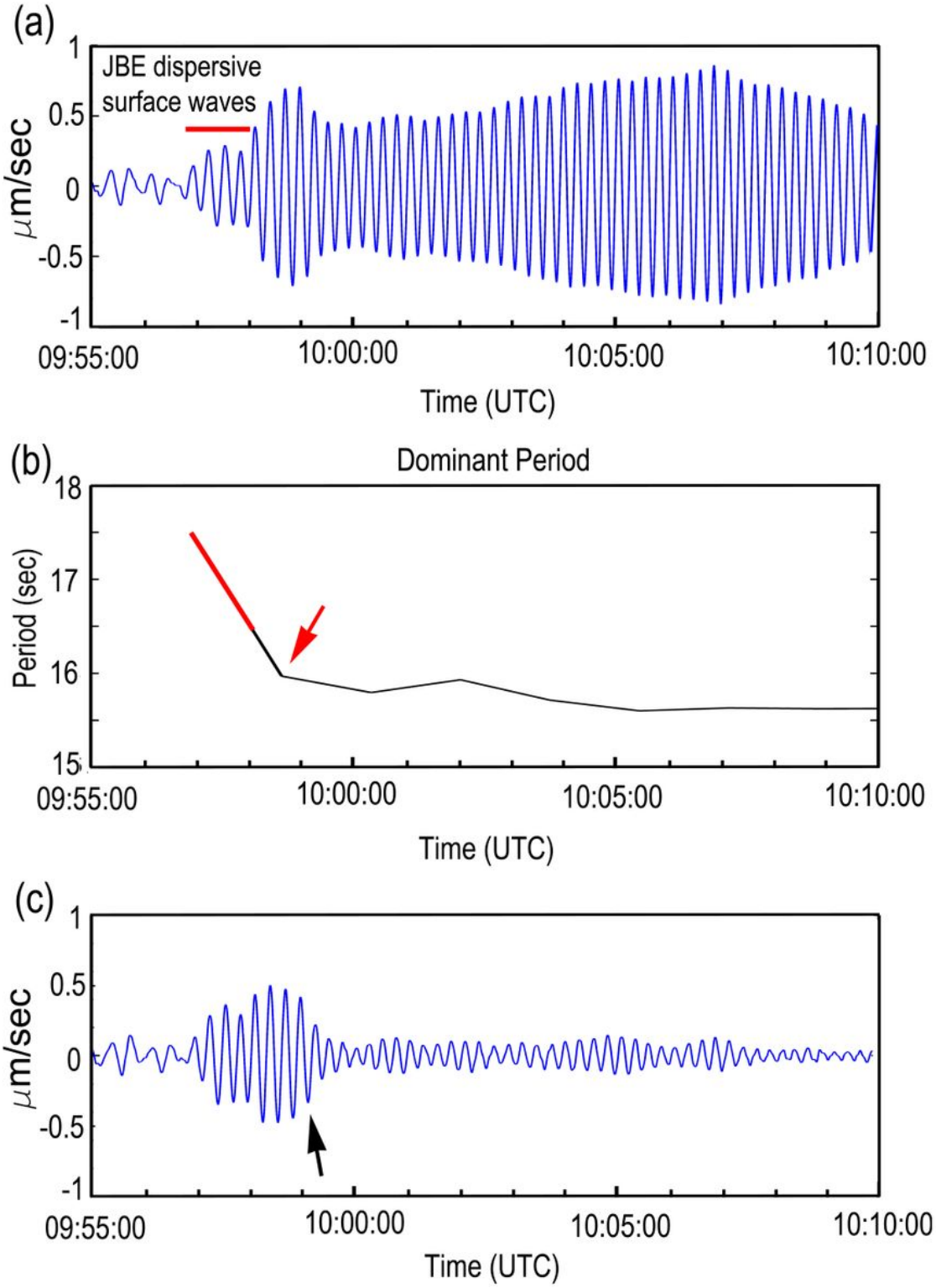

Figure 10

(a) is the same as the latter half of the top of Figure 3. Waveforms of JBE (Just Before the monochromatic Event) and SEQ can be seen. (b) shows the dominant periods of the waveforms in figure (a). The dispersion of the surface waves is clear, and in the range of periods from 17.5 to 16.5 sec is visible in the waveform (marked by red). The red arrow indicates 09:58:38 UTC. (c) shows notch filter

output of the waveform with the notch in the period of 15.6 sec and the bandwidth of 1 sec. The black arrow indicates 09:59:09 UTC.

Supplementary Files

This is a list of supplementary files associated with this preprint. Click to download.

- Appendix.docx
- Graphicalabstract.jpg